PAX8–GLIS3 gene fusion is a pathognomonic genetic alteration of hyalinizing trabecular tumors of the thyroid

PAX8-GLIS3 GENE FUSION IS A PATHOGNOMONIC GENETIC ALTERATION OF HYALINIZING TRABECULAR TUMOR OF THE THYROID

Running title: *PAX8-GLIS3* fusion in thyroid neoplasms.

Caterina Marchiò[1,2]§, Arnaud Da Cruz Paula[3]§, Rodrigo Gularte-Merida[4], Thais Basili[4], Alissa Brandes[4], Edaise M. da Silva[4], Catarina Silveira[4], Lorenzo Ferrando[4,5], Jasna Metovic[6], Francesca Maletta[6], Laura Annaratone[1,2], Fresia Pareja[4], Brian P. Rubin[7], Aaron P. Hoschar[7], Giovanni De Rosa[8], Stefano La Rosa[9], Massimo Bongiovanni[9], Bibianna Purgina[10], Simonetta Piana[11], Marco Volante[12], Britta Weigelt[4], Jorge S. Reis-Filho[4,13]#, Mauro Papotti[6]#

[1]FPO-Candiolo Cancer Institute, Candiolo, Italy

[2]Department of Medical Sciences, University of Turin, Torino, Italy

[3]Department of Surgery, Memorial Sloan Kettering Cancer Center, New York, NY, USA

[4]Department of Pathology, Memorial Sloan Kettering Cancer Center, New York, NY, USA

[5]Department of Internal Medicine, University of Genoa, Genoa, Italy

[6]Department of Oncology, University of Turin, at Città della Salute Hospital, Torino, Italy

[7]Department of Pathology, Cleveland Clinic, Cleveland, OH, USA

[8]Pathology Division, Mauriziano Hospital, Torino, Italy

[9]Service of Clinical Pathology, Lausanne University Hospital, Institute of Pathology, Lausanne, Switzerland

[10]Department of Pathology and Laboratory Medicine, Ottawa Hospital, Ontario, Canada

[11]Pathology Unit, Arcispedale Santa Maria Nuova, Azienda USL-IRCCS Reggio Emilia, Italy

[12]San Luigi Gonzaga Hospital and Department of Oncology, University of Turin, Orbassano, Italy

[13]Human Oncology and Pathogenesis Program, Memorial Sloan Kettering Cancer Center, New York, NY, USA

[§]*These authors equally contributed to this work.*

[#]*These authors jointly directed the work.*

Correspondence to:

Prof. Mauro Papotti, Department of Oncology, University of Turin, at Città della Salute Hospital, via Santena 7, 10126, Torino, Italy. Phone: +39 011 670 5800. Email: mauro.papotti@unito.it.

Dr. Jorge S. Reis-Filho, MD PhD FRCPath, Department of Pathology, Memorial Sloan Kettering Cancer Center, 1275 York Avenue, New York, NY 10065, USA. Phone: +1 212 639 8054. Email: reisfilj@mskcc.org.

ABSTRACT

Hyalinizing trabecular adenoma/tumor (HTT) is a rare and poorly characterized follicular-derived thyroid neoplasm recently shown to harbor recurrent *PAX8*-G*LIS1* or *PAX8*-*GLIS3* gene fusions. Here we sought to define the repertoire of genetic alterations of HTTs, and whether *PAX8*-G*LIS3* fusions are pathognomonic for HTTs. A discovery series of 8 HTTs was subjected to RNA-sequencing (n=8), whole-exome sequencing (n=3) or targeted massively parallel sequencing (n=5). No recurrent somatic mutations or copy number alterations were identified in HTT, whereas RNA-sequencing revealed the presence of a recurrent genetic rearrangement involving *PAX8* (2q14.1) and *GLIS3* (9p24.2) genes in all cases. In this in-frame fusion gene, which comprised exons 1-2 of *PAX8* and exons 3-11 of *GLIS3, GLIS3* is likely placed under the regulation of *PAX8*. Reverse transcription (RT)-PCR and/or fluorescence *in situ* (FISH) analyses of a validation series of 26 HTTs revealed that the *PAX8*-*GLIS3* gene fusion was present in all HTTs (100%). No *GLIS1* rearrangements were identified. Conversely, no *PAX8*-G*LIS3* gene fusions were detected in a cohort of 237 control thyroid neoplasms, including 15 trabecular thyroid lesions highly resembling HTT from a morphological standpoint, as well as trabecular/solid follicular adenomas, solid/trabecular variants of papillary carcinoma, and Hurthle cell adenomas or carcinomas. Our data provide evidence to suggest that the *PAX8*-*GLIS3* fusion is pathognomonic for HTTs, and that the presence of the *PAX8*-*GLIS3* fusion in thyroid neoplasms may be used as an ancillary marker for the diagnosis of HTT, thereby avoiding overtreatment in case of misdiagnoses with apparently similar malignant tumors.

KEY WORDS: hyalinizing trabecular tumor, thyroid, PAX8, GLIS3, gene fusion, differential diagnosis.

INTRODUCTION

Hyalinizing trabecular adenoma/tumor (HTT) is a rare follicular-derived, thyroglobulin producing, thyroid neoplasm composed of large trabeculae of elongated or polygonal eosinophilic cells admixed with intratrabecular hyaline material of the basal membrane type. HTT shares many nuclear features of those of papillary thyroid carcinoma (PTC), namely nuclear clearing, grooves, pseudoinclusions and irregular borders (1). This tumor was described as a benign follicular tumor (a single malignant case is on record among 118 benign HTTs reviewed some years ago) (2, 3) and was variably named, as either adenoma or tumor or neoplasm of uncertain malignant potential. No etiological or risk factors are known for HTT and a real understanding of its nature is missing (2). An association with PTC is reported in up to 5% of cases and HTT itself has been related to PTC based on shared morphological features and *RET* gene alterations in a fraction of cases (4, 5). Besides *RET-PTC* rearrangements, no other PTC-related genetic abnormalities, such as *BRAF* mutations (6) or microRNA expression (7, 8), have been described in association with HTT. Similarly, no follicular tumor–related alterations were found, including *RAS* gene mutations or *PAX8-PPARgamma* rearrangements, the latter originally claimed to be specific of follicular carcinomas (9).

Very recently, Nikiforova and co-workers (10) have reported on the presence of gene fusions involving *PAX8* and *GLIS* genes as pathognomonic genomic features underlying HTT. These fusions, in particular the *PAX8–GLIS3* rearrangement, were identified in 100% of tumors with cardinal unequivocal morphological and immunophenotypical features of HTT. By performing a thorough genomic characterization of this entity, the same authors were also able to show that HTT typically shows a quiet genome with a low number of somatic mutations and no significant DNA copy number alterations (10).

In this study, we provide a thorough independent validation of the presence of the *PAX8–GLIS3* fusion in a large multi-institutional series of 34 HTTs, as opposed to its absence in 237 control thyroid neoplasms that also included 15 trabecular tumors of follicular derivation highly resembling HTT from a morphological standpoint, thus posing a potential diagnostic interpretational issue in both histopathologic and fine needle aspiration cytology diagnostic practice.

MATERIAL AND METHODS

Cases

After obtaining approval by the IRBs and local research ethics committees from the authors' institutions, the pathology files of the authors' institutions (Città della Salute Hospital and Mauriziano Hospital in Torino, Italy; San Luigi Hospital in Orbassano-Torino, Italy; Service of Clinical Pathology, Lausanne University Hospital, Switzerland; IRCCS in Reggio Emilia, Italy; Cleveland Clinic, Ohio, USA; Ottawa Hospital, Canada) were searched for a diagnosis of either "hyalinizing trabecular tumor" or "hyalinizing trabecular adenoma" of the thyroid. Samples were anonymized prior to the analyses. Representative hematoxylin & eosin (H&E) and Ki67/MIB1 stained slides of 38 HTTs were centrally reviewed by two pathologists with a expertise in thyroid neoplasms (MV and MP). The diagnosis of HTT was based on the strict diagnostic criteria reported in the WHO classification of endocrine tumors of the thyroid (1), as well as in previous publications (11, 12). Upon pathological review, 34 cases were unanimously diagnosed as HTT; four cases were excluded and reclassified as follicular adenomas of the trabecular or Hurthle cell type (three tumors: # 13T, 15T, 23T) and as Hurthle cell carcinoma based on signs of vascular invasion in the remaining case (# 24T) (Figure 1).

Of the 34 HTTs included in this study, four (HTT02, HTT06, HTT12, HTT33) also contained a small, classical PTC in the same thyroid lobe, but topographically independent from the HTT nodule. In addition, a separate series of 237 neoplasms that represented a comprehensive landscape of thyroid lesions were used as controls, and comprised 119 PTCs, 24 follicular carcinomas, 13 poorly differentiated carcinomas, 25 anaplastic carcinomas, 15 medullary carcinomas, 18 Hurthle cell tumors, and 23 follicular adenomas (Figure 1). Within this series, 15 tumors showed morphological features highly reminiscent of HTT, i.e. prominent solid/trabecular growth pattern and more or less extensive hyalinization. These were appropriately classified in different categories (i.e. follicular adenomas of trabecular/embryonal variant, solid/trabecular variant of papillary carcinomas, Hurthle cell adenomas, Hurthle cell carcinoma).

First, eight HTTs were subjected as a discovery series to RNA- and DNA-sequencing (Figure 1). Subsequently, a validation series of 26 HTTs were subjected to reverse transcription (RT)-PCR and fluorescence *in situ* (FISH) analyses (Figure 1).

Microdissection and nucleic acid extraction

Eight-micron-thick sections were cut from formalin fixed paraffin embedded (FFPE) blocks of the tumor and normal thyroid tissue, stained with nuclear fast red and microdissected under a stereomicroscope as previously described (13) to ensure >80% of tumor cells content and that the normal tissue was devoid of neoplastic cells. RNA and genomic DNA were extracted and quantified as previously described (14).

Immunohistochemistry

Four-micron-thick sections were cut from the representative FFPE block of each HTT and processed for Ki67 immunohistochemistry with an automatic immunostainer (Ventana BenchMark AutoStainer, Ventana Medical Systems, Tucson, USA), with the exception of the primary antibody incubation step, which was manually performed at room temperature for 30 minutes using the Ki67 clone MIB1 (Dako/Agilent, Glostrup, Denmark) diluted 1/50, after antigen retrieval with the commercial Ventana CC1 solution for 36 minutes. The evaluation of Ki67 relied on a qualitative assessment of the staining pattern of staining (membranous versus nuclear).

Whole-exome and targeted massively parallel sequencing

Microdissected tumor and normal DNA samples from eight HTTs (discovery set) were subjected to whole-exome sequencing (WES, n=3) (15) and to Memorial Sloan Kettering-Integrated Mutation Profiling of Actionable Cancer Targets (MSK-IMPACT) sequencing (n=5; Figure 1), which targets all exons and selected introns of 410 cancer genes, as previously described (16, 17) (Supplementary Table S1). Three additional cases from the validation set were also subjected to MSK-IMPACT (Figure 1).

Analysis of sequencing data was performed as previously described (15, 17). In brief, somatic single-nucleotide variants (SNVs) were detected using MuTect (v1.0) (18), and small insertion and deletions (indels) by Strelka (v2.0.15) (19), VarScan2 (v2.3.7) (20), Lancet (v1.0.0) (21) and Scalpel (v0.5.3) (22). SNVs and indels for which the tumor mutant allele fraction (MAF) was <5 times that of the matched normal MAF were excluded. SNVs and indels found at >1% global

minor allele frequency in ExAC (23), as well as common SNPs reported in dbSNP (build 150) were also excluded. Copy number alterations (CNAs) and loss of heterozygosity (LOH) were defined using FACETS (24). ABSOLUTE (v1.0.6) (25) was employed to determine the cancer cell fraction (CCF) of each mutation, as previously described (15, 17). A mutation was classified as clonal if its probability of being clonal was >50% or if the lower bound of the 95% confidence interval of its CCF was >90%, as previously described (15, 17). Mutations affecting hotspot codons were annotated according to Chang et al (26).

RNA-sequencing and fusion gene identification

RNA-sequencing was performed on eight HTTs (Figure 1, Supplementary Table S1) using validated protocols (15) employed at MSKCC's Integrated Genomics Operation (IGO). In brief, paired-end RNA-sequencing was performed with 2 × 50 bp cycles on an Illumina HiSeq2000. Read pairs supporting fusion transcripts were identified using INTEGRATE (27), deFuse (28) and FusionCatcher (29), as previously described (15, 30). To account for alignment artifacts and normal transcriptional variants, we excluded fusion gene and read-through candidates that were also identified in a set of 297 normal samples from TCGA (31). The remaining in-frame candidate fusion genes were annotated using OncoFuse (32) to define their likelihood of constituting potential driver fusion genes. The presence of the in-frame candidate fusion genes identified was also assessed across 33 cancer types in the tumor fusion gene data portal (33) which comprises a list of 20,231 fusion genes.

***PAX8-GLIS3* FISH analysis**

PAX8-GLIS3 fusion gene assessment by FISH was performed using validated protocols at MSKCC's Molecular Cytogenetics Core, as previously described (34). Three-color *PAX8-GLIS3* probe were employed, consisting of bacterial artificial chromosomes (BACs) mapping to 5'*PAX8* (green), 3'*PAX8* (red) and 3'*GLIS3* (orange). At least ten images per tumor region were captured and at least 50 non-overlapping interphase nuclei with well-delineated contours were analyzed for the presence of the *PAX8-GLIS3* fusion. HTTs were considered positive for the *PAX8-GLIS3* fusion gene if >15% of the cells displayed at least one 5'*PAX8*-3'*GLIS3* fusion signal.

Reverse Transcription-PCR (RT-PCR)

Total RNA was reverse-transcribed using SuperScript Vilo Master Mix (Life Technologies; Thermo Fisher Scientific), according to the manufacturer's instructions. PCR amplification of 10ng of cDNA was performed using specific primer sets designed based on the known fusion genes and breakpoints (Supplementary Table S2). PCR fragments were purified (ExoSAP-IT, Affymetrix) and sequenced on an ABI 3730 capillary sequencer using the ABI BigDye Terminator chemistry (v3.1, Life Technologies) according to the manufacturer's protocol. Sequences of the forward and reverse strands were analyzed using MacVector software (MacVector, Inc., Cary, NC, USA). All analyses were performed in duplicate.

RESULTS

Histologic features

All 34 HTTs included in this study displayed the cardinal morphological features of HTT: a growth pattern made of thick trabeculae; elongated or -more rarely- polygonal cells arranged with a perpendicular orientation compared to the trabecular axis; eosinophilic cytoplasm and clear nuclei with irregular borders, grooves and pseudoinclusions; and finally presence of more or less abundant intratrabecular hyaline material often embedding single or groups of tumor cells (Figure 2). In addition, all HTTs displayed immunoreactivity at the cell membrane for the MIB1 monoclonal antibody to Ki67 (Figure 2).

The 237 control cases, whose histology is detailed in Supplementary Table S3, had the expected morphology for each single tumor entity, with the exception of 15 selected cases that had a prominent solid and/or trabecular growth pattern and more or less extensive signs of hyalinization that resembled HTT, but were eventually classified as variants of follicular adenoma (trabecular/embryonal variant, n=8), Hurthle cell adenoma (solid/trabecular patterns, n=2), papillary carcinoma (solid/trabecular variant, n=3), Hurthle cell carcinoma (solid/trabecular patterns, n=1) and poorly differentiated carcinoma (trabecular variant, n=1) (Figure 1). In all such cases, an HTT was originally suspected or diagnosed, based on the trabecular growth pattern and the presence of stromal hyaline material. The trabeculae were generally thin and merged,

however, with compact solid nests made of cells haphazardly oriented along the axis of the cords (rather than perpendicularly) and with a deeply eosinophilic and granular cytoplasm, as commonly seen in Hurthle cells neoplasms. In addition and more importantly, the variable degree of hyaline material was in any case restricted to the space between the trabeculae and was not distributed inside them (with the tight contact to neoplastic cells typically observed in HTT). Finally, in all other thyroid neoplasms included the diagnosis of HTT was not supported due to the lack of the peculiar cell membrane reactivity pattern for Ki67/MIB1 (Figure 3).

Mutational landscape and copy number alterations in HTT

To assess the somatic genetic alterations, three and eight cases were subjected to WES (median depth of coverage of tumor 139x (range 137x-164x), and normal 151x (range 131x-161x) samples) and targeted MSK-IMPACT sequencing (median depth of coverage of tumor 311x (range 18x-499x), and normal 174x (range 41x-530x) samples), respectively (Supplementary Table S4).

HTTs displayed a low tumor burden, with a median of 16 (range 10-22) somatic mutations defined by WES, of which 11 (range 9-19) were non-synonymous, while the MSK-IMPACT assay detected a median of 1 (range 1-2) somatic mutations of which 1 (range 1-2) were non-synonymous. No recurrent somatic mutations were identified in the HTTs analyzed. The majority of mutations were non-pathogenic missense mutations not affecting hotspot residues, and four HTTs subjected to MSK-IMPACT sequencing did not harbor any mutations affecting the 410 cancer-related genes tested (Supplementary Figure S1). The potentially pathogenic non-synonymous mutations identified included a subclonal *FIP1L1* (p.L26R) missense mutation and a clonal *ITK* (p.R581W) missense mutation in HTT10 and HTT11, respectively. Analysis from MSK-IMPACT demonstrated a subclonal *SPEN* (p.P1892Qfs*6) frameshift mutation and a clonal *KDM5A* (p.R719H) missense mutation in HTT01, and a subclonal *TP63* (p.X549) splice site mutation in HTT08 (Supplementary Figure S1, Supplementary Table S5).

Genome copy number analysis revealed a diploid/near-diploid genome in the 11 HTTs analyzed in this study (Supplementary Figure S2). No homozygous deletions or high-level amplifications were found in the HTTs analyzed.

PAX8-GLIS3 fusion detection and validation in HTT

Based on the initial findings of a quiet genome and lack of recurrent pathogenic somatic mutations, the eight HTTs of our discovery series were subjected to global RNA-sequencing analysis, which detected the presence of a recurrent, in-frame *PAX8-GLIS3* fusion gene (8/8, 100%), resulting in a chimeric transcript composed of exons 1-2 of *PAX8* and exons 3-11 of *GLIS3* (Figure 4A, Supplementary Table S2). The fusion of exons 1-2 of *PAX8* to the 3'-end of *GLIS3* results in the increased expression of exons 3-11 of *GLIS3*, as assessed using the RPKM counts (Figure 4B). In the eight HTTs and in validation series of 26 HTTs, the *PAX8-GLIS3* fusion gene was confirmed/ present by FISH (*n*=12) and/or RT-PCR (*n*=33) in all HTTs (100%; Figure 4C-D, Supplementary Table S3). Four HTTs had a concurrent PTCs, and whilst the *PAX8-GLIS3* fusion gene was present in the HTT, it was absent in the PTCs of these cases (Figure 5).

Lack of *PAX8-GLIS3* fusions in thyroid neoplasms

To determine whether *PAX8-GLIS3* rearrangements would constitute a pathognomonic genetic alteration in the HTTs, FISH and RT-PCR were performed in the series of 237 control cases, which included the whole spectrum of conventional thyroid neoplasms and also encompassed a subgroup of 15 tumors of follicular derivation characterized by a prominent trabecular growth and hyalinization that was reminiscent of HTT on sole morphological ground. None of these controls and potential differential diagnoses of HTT harbored the *PAX8-GLIS3* rearrangement (Figure 4E, Supplementary Table S3). In addition, none of the 9,950 tumors from 33 cancer types from The Cancer Genome Atlas (33) were found to harbor the specific *PAX8-GLIS3* fusion (Figure 4F). These data provide evidence to suggest that the *PAX8-GLIS3* fusion is pathognomonic for HTTs.

DISCUSSION

Here we present a validation of the recently reported *PAX8-GLIS3* rearrangement (10) as a hallmark genomic feature of the rare hyalinizing trabecular tumor (HTT) of the thyroid. In agreement with Nikiforova et al. findings (10), all of the 34 histologically proven HTTs of the

present study harbored the *PAX8-GLIS3* fusion. This gene rearrangement has been consistently demonstrated by different techniques, using specifically designed probes, which confirmed the occurrence of such rearrangement. In parallel, this fusion gene was not present in control thyroid tumors of various histologies, including an interesting series of trabecular tumors of follicular derivation that was specifically selected from our files for the purpose of testing the power of this novel fusion, as a potential differential diagnostic marker.

The origin of HTT is unknown. No risk factors have so far been reported and the claimed relationship with PTC had been challenged by the absence of *BRAF* mutations (6), and now definitely excluded by the specific *PAX8-GLIS3* rearrangement (or *PAX8-GLIS1,* as reported by Nikiforova et al. (10)), that never occurred in the 300 papillary cancers so far analyzed in published (10) and in the present series, with one exception in the Nikiforova's series (10) and in the TGCA series of 484 PTCs (35). The case regarded a trabecular tumor focally reminiscent of HTT that was eventually diagnosed as a PTC and probably represents the same case used in the two different publications (10). With regard to follicular adenoma and carcinoma, the similarities with HTT are even more scant on both morphological and genetic grounds. Besides *RAS* gene mutations, follicular adenomas and carcinomas were found to harbor a rearrangement of *PAX8-PPARgamma* genes that was originally reported to be restricted to malignant conditions, only (9), but subsequently identified also in a fraction of follicular adenomas, although never in HTT. Interestingly, the novel HTT-specific fusion is also correlated to the *PAX8* gene, although the fusion occurred with another locus, mapping to chromosome 9p24.2 to produce the *PAX8-GLIS3* rearrangement, or to chromosome 1 in the case of the rarer *GLIS1* type fusion (10).

Although the newly discovered genetic alteration may not bear any impact in the therapeutic strategy of the patients, since surgery is generally sufficient to cure the tumor, the novel fusion product represents a relevant diagnostic tool of this rare tumor in surgical samples and, in particular, in preoperative cytology specimens, in which the diagnosis of HTT is reached in no more than 8% of cases (36). In fact, the differential diagnosis from solid/trabecular variants of papillary carcinoma may occasionally pose problems due to the overlapping nuclear features of the two tumors, while genetically the two entities seem unrelated with a predominance of *BRAF* and *RAS* gene mutations in papillary cancer, but not in HTT (6). In addition, even follicular

neoplasms may resemble HTT when the growth pattern is predominantly trabecular or solid, as seen in embryonal/fetal type follicular adenomas or in poorly differentiated carcinomas. The commonly shared thyroglobulin production is of no help in this setting of differential diagnosis, and the only useful HTT marker is the peculiar membrane pattern (artefactually) produced by Ki67 immunostaining, provided specific technical conditions are met (i.e. use of MIB1 monoclonal and room temperature incubation), in order to obtain the expected cell membrane reactivity (37).

Although diagnostic criteria for both HTT and its mimickers are apparently clear-cut, it is the experience of some of us that in the daily consultation practice, a certain degree of confusion exists among the different entities. The major source of controversies is the presence of more or less hyalinized stroma in an otherwise trabecular or solid/compact tumor cell proliferation of follicular derivation. Such a pattern of growth is shared by several primary tumors of various nature, including not only follicular tumors (embryonal adenoma, solid variant of papillary carcinoma, Hurthle cell neoplasms, poorly differentiated carcinoma), but also by medullary carcinoma and intrathyroid parathyroid tumors. Apart from the differences in cell type and -obviously- in the ultimate immunoprofile of tumor cells, the trabecular structure is crucial for a diagnosis of HTT: thick cords of elongated cells, arranged perpendicular to the major axis of the trabecula itself, contain variable amounts of hyaline collagenized material inside the trabeculae, to surround individual tumor cells. The general impression is that of a paraganglioma rather than a trabecular follicular derived tumor, but the extent of hyalinization may change the overall picture and cause misdiagnoses. Indeed, all 15 trabecular cases, including 4 originally submitted as HTT, that we deliberately selected among the control cases lacked the *PAX8-GLIS3* fusion. This supports the notion that the spectrum of trabecular thyroid neoplasms is relatively wide and heterogeneous, including a variety of growth patterns in which thick trabeculae merge with hyaline material depicting in the end more than one specific follicular derived, benign or malignant, entity or subtype. The novel described *PAX8-GLIS3* fusion is a valuable hint to take HTT apart from its mimickers.

Interestingly, four HTT cases had associated small papillary carcinomas, which did not harbor the *GLIS3* fusion product. In addition, in the Nikiforova's study (10) a link with upregulation of genes implicated in collagen type IV deposition was suggested, as the result of

the gene rearrangement involving chromosomes 2 and 9, although the exact mechanisms remain to be elucidated. The abundance of basal membrane type material included collagen IV had been reported in prior immunohistochemical studies by Li and Rosai (38) and Papotti and co-workers (12). These molecular and morphological findings may be of further help in taking apart real HTT from all the mimickers discussed above, care being taken to identify a predominant intratrabecular collagen deposition (rather than in the neoplastic stroma), since such a material seems to be the direct result of collagen-related gene upregulation in the fusion-positive neoplastic cells.

Finally, as demonstrated by Nikiforova and co-workers using ThyroSeq v3 gene panel in over 10,000 FNABs (10, 39), this novel fusion may represent a relevant diagnostic marker of HTT in preoperative fine needle aspiration biopsies, especially to take it apart from other solid/trabecular thyroid tumors with prominent hyalinization. A correct preoperative characterization of HTT can result from molecular methods or from immunohistochemistry for GLIS3, to refrain from unnecessary surgery of indeterminate cytology trabecular/follicular nodules harboring the *PAX8-GLIS3* fusion.

In conclusion, HTT represents a unique tumor based on its morphological (intratrabecular hyalinization, papillary cancer-like nuclei), immunohistochemical (Ki67/MIB1 expression at the cell membrane) and now also molecular (*PAX8-GLIS3* fusion) features. The latter support the notion of separately classifying this tumor, as originally proposed by Carney (11), taking it apart from both papillary carcinomas and the other conventional follicular thyroid neoplasms.

Acknowledgements: This work was supported by grants from the Associazione Italiana Ricerca sul Cancro (AIRC, Milan, No. IG 20100 to MP), the Italian Ministry of Education, University and Research (MIUR ex-60%-2017, 2015HAJH8E and FPRC 5xmille 2015 MIUR-“Progetto Futuro” to CM). LA is funded by Fondazione Umberto Veronesi. We acknowledge also funding by MIUR project “Dipartimenti di Eccellenza 2018-2022” (Project no. D15D18000410001) to the Department of Medical Sciences of the University of Turin, Italy.

JSR-F is funded by Breast Cancer Research Foundation. Research reported in this publication was funded in part by a Cancer Center Support Grant of the National Institutes of Health/National Cancer Institute (grant No P30CA008748). The content is solely the responsibility of the authors and does not necessarily represent the official views of the National Institutes of Health.
The funders of this study had no role in the design of the study; the collection, analysis, and interpretation of the data; the writing of the manuscript; and the decision to submit the manuscript for publication.

Disclosure/Conflict of Interest: CM has received personal/consultancy fees from Axiom Healthcare Strategies, Daiichi-Sankyo, and Bayer, outside the scope of the submitted work. JSR-F reports personal/consultancy fees from VolitionRx, Page.AI, Goldman Sachs, Grail, Ventana Medical Systems, Roche and Genentech, outside the scope of the submitted work. All remaining authors have no conflicts of interest to declare.

REFERENCES

1. Papotti M, Volante M. Hyalinizing trabecular tumor, In: Lloyd RVeae, (ed). WHO classification of tumors of endocrine organs. IARC Press: Lyon. pp 73-4.

2. Carney JA, Hirokawa M, Lloyd RV, Papotti M, Sebo TJ. Hyalinizing trabecular tumors of the thyroid gland are almost all benign. Am J Surg Pathol 2008;32:1877-89.

3. Gowrishankar S, Pai SA, Carney JA. Hyalinizing trabecular carcinoma of the thyroid gland. Histopathology 2008;52:529-31.

4. Cheung CC, Boerner SL, MacMillan CM, Ramyar L, Asa SL. Hyalinizing trabecular tumor of the thyroid: a variant of papillary carcinoma proved by molecular genetics. Am J Surg Pathol 2000;24:1622-6.

5. Papotti M, Volante M, Giuliano A*, et al.* RET/PTC activation in hyalinizing trabecular tumors of the thyroid. Am J Surg Pathol 2000;24:1615-21.

6. Salvatore G, Chiappetta G, Nikiforov YE*, et al.* Molecular profile of hyalinizing trabecular tumours of the thyroid: high prevalence of RET/PTC rearrangements and absence of B-raf and N-ras point mutations. Eur J Cancer 2005;41:816-21.

7. Sheu SY, Vogel E, Worm K*, et al.* Hyalinizing trabecular tumour of the thyroid-differential expression of distinct miRNAs compared with papillary thyroid carcinoma. Histopathology 2010;56:632-40.

8. Acquaviva G, Visani M, Repaci A*, et al.* Molecular pathology of thyroid tumours of follicular cells: a review of genetic alterations and their clinicopathological relevance. Histopathology 2018;72:6-31.

9. Kroll TG, Sarraf P, Pecciarini L*, et al.* PAX8-PPARgamma1 fusion oncogene in human thyroid carcinoma Science 2000;289:1357-60.

10. Nikiforova MN, Nikitski AV, Panebianco F*, et al.* GLIS Rearrangement is a Genomic Hallmark of Hyalinizing Trabecular Tumor of the Thyroid Gland. Thyroid 2019;29:161-73.

11. Carney JA, Ryan J, Goellner JR. Hyalinizing trabecular adenoma of the thyroid gland. Am J Surg Pathol 1987;11:583-91.

12. Papotti M, Riella P, Montemurro F, Pietribiasi F, Bussolati G. Immunophenotypic heterogeneity of hyalinizing trabecular tumours of the thyroid. Histopathology 1997;31:525-33.

13. Marchio C, Geyer FC, Ng CK*, et al.* The genetic landscape of breast carcinomas with neuroendocrine differentiation. J Pathol 2017;241:405-19.

14. Guerini-Rocco E, Hodi Z, Piscuoglio S*, et al.* The repertoire of somatic genetic alterations of acinic cell carcinomas of the breast: an exploratory, hypothesis-generating study. J Pathol 2015;237:166-78.

15. Pareja F, Lee JY, Brown DN*, et al.* The Genomic Landscape of Mucinous Breast Cancer. J Natl Cancer Inst 2019.

16. Zehir A, Benayed R, Shah RH*, et al.* Mutational landscape of metastatic cancer revealed from prospective clinical sequencing of 10,000 patients. Nat Med 2017;23:703-13.

17. Geyer FC, Li A, Papanastasiou AD*, et al.* Recurrent hotspot mutations in HRAS Q61 and PI3K-AKT pathway genes as drivers of breast adenomyoepitheliomas. Nat Commun 2018;9:1816.

18. Cibulskis K, Lawrence MS, Carter SL*, et al.* Sensitive detection of somatic point mutations in impure and heterogeneous cancer samples. Nat Biotechnol 2013;31:213-9.

19. Saunders CT, Wong WS, Swamy S*, et al.* Strelka: accurate somatic small-variant calling from sequenced tumor-normal sample pairs. Bioinformatics 2012;28:1811-7.

20. Koboldt DC, Zhang Q, Larson DE*, et al.* VarScan 2: somatic mutation and copy number alteration discovery in cancer by exome sequencing. Genome Res 2012;22:568-76.

21. Narzisi G, Corvelo A, Arora K*, et al.* Genome-wide somatic variant calling using localized colored de Bruijn graphs. Commun Biol 2018;1:20.

22. Narzisi G, O'Rawe JA, Iossifov I*, et al.* Accurate de novo and transmitted indel detection in exome-capture data using microassembly. Nat Methods 2014;11:1033-6.

23. Lek M, Karczewski KJ, Minikel EV*, et al.* Analysis of protein-coding genetic variation in 60,706 humans. Nature 2016;536:285-91.

24. Shen R, Seshan VE. FACETS: allele-specific copy number and clonal heterogeneity analysis tool for high-throughput DNA sequencing. Nucleic Acids Res 2016;44:e131.

25. Carter SL, Cibulskis K, Helman E*, et al.* Absolute quantification of somatic DNA alterations in human cancer. Nat Biotechnol 2012;30:413-21.

26. Chang MT, Bhattarai TS, Schram AM*, et al.* Accelerating Discovery of Functional Mutant Alleles in Cancer. Cancer Discov 2018;8:174-83.

27. Zhang J, White NM, Schmidt HK*, et al.* INTEGRATE: gene fusion discovery using whole genome and transcriptome data. Genome Res 2016;26:108-18.

28. McPherson A, Hormozdiari F, Zayed A*, et al.* deFuse: an algorithm for gene fusion discovery in tumor RNA-Seq data. PLoS Comput Biol 2011;7:e1001138.

29. Edgren H, Murumagi A, Kangaspeska S*, et al.* Identification of fusion genes in breast cancer by paired-end RNA-sequencing. Genome Biol 2011;12:R6.

30. Piscuoglio S, Burke KA, Ng CK*, et al.* Uterine adenosarcomas are mesenchymal neoplasms. J Pathol 2016;238:381-8.

31. Cancer Genome Atlas N. Comprehensive molecular portraits of human breast tumours. Nature 2012;490:61-70.

32. Shugay M, Ortiz de Mendibil I, Vizmanos JL, Novo FJ. Oncofuse: a computational framework for the prediction of the oncogenic potential of gene fusions. Bioinformatics 2013;29:2539-46.

33. TUMOR FUSION GENE DATA PORTAL. http://www.tumorfusions.org. Accessed: March 2019.

34. Martelotto LG, De Filippo MR, Ng CK*, et al.* Genomic landscape of adenoid cystic carcinoma of the breast. J Pathol 2015;237:179-89.

35. Cancer Genome Atlas Research N. Integrated genomic characterization of papillary thyroid carcinoma. Cell 2014;159:676-90.

36. Saglietti C, Piana S, La Rosa S, Bongiovanni M. Hyalinizing trabecular tumour of the thyroid: fine-needle aspiration cytological diagnosis and correlation with histology. J Clin Pathol 2017;70:641-7.

37. Leonardo E, Volante M, Barbareschi M*, et al.* Cell membrane reactivity of MIB-1 antibody to Ki67 in human tumors: fact or artifact? Appl Immunohistochem Mol Morphol 2007;15:220-3.

38. Li M, Carcangiu ML, Rosai J. Abnormal intracellular and extracellular distribution of basement membrane material in papillary carcinoma and hyalinizing trabecular tumors of the thyroid: implication for deregulation of secretory pathways. Hum Pathol 1997;28:1366-72.

39. Nikiforova MN, Mercurio S, Wald AI*, et al.* Analytical performance of the ThyroSeq v3 genomic classifier for cancer diagnosis in thyroid nodules. Cancer 2018;124:1682-90.

FIGURE LEGENDS

Figure 1: Schematic representation of the tissue samples and sequencing methods employed in this study. Depiction of the discovery and of the validation series of hyalinizing trabecular tumors (HTTs) of the thyroid, and the comprehensive series of other thyroid neoplasms here investigated, including 15 cases (*) in which the morphological features were highly reminiscent of an HTT. The sequencing analysis methods utilized in each cohort are detailed.

Figure 2: Representative micrographs of hyalinizing trabecular tumors of the thyroid. A 3 mm large well-circumscribed HTT (**A**) showing tumor cells arranged in trabeculae and small nests with abundant intratrabecular hyaline material (**B**), and another classical case of HTT (**C**) showing elongated and spindle cells with nuclear palisading and hyaline material in the background displaying the unique cell membrane reactivity with the MIB1 monoclonal antibody against Ki67 (**D**).

Figure 3. Representative micrographs of thyroid neoplasms mimicking HTTs. The figure illustrates a follicular adenoma of trabecular variant (**A**, 200x), a poorly differentiated thyroid carcinoma (**B**, 200x), and a Hurthle cell carcinoma (**C**, 200x) with prominent hyalinization, mimicking HTT on morphological ground. No membrane Ki67/MIB1 staining was observed, as exemplified here for the case of follicular thyroid adenoma with trabecular features (**D**, 200x).

Figure 4: Recurrent *PAX8-GLIS3* fusion gene in hyalinizing trabecular tumors of the thyroid. A) Schematic representation of the *PAX8-GLIS3* fusion transcript including the exons and domains involved. The breakpoint of the 5' and 3' partner genes are represented as black vertical lines. Spanning reads are depicted and aligned to the predicted junction sequence. **B)** Schematic representation showing the Reads Per Kilobase per Million (RPKM) mapped read counts of each exon of *GLIS3*. The *GLIS3* fusion breakpoint is represented as a red dashed line. **C)** Representative micrographs of fluorescent *in situ* hybridization (FISH) for *PAX8-GLIS3*. **D)** Representative Sanger sequencing electropherograms of the genomic *PAX8-GLIS3* breakpoint

(Top) and frequency of *PAX8-GLIS3* fusion gene in HTTs involved in this study determined by RT-PCR (bottom). **E)** Representative micrograph of fluorescent *in situ* hybridization (FISH) for the absence of *PAX8-GLIS3* (top) and frequency of *PAX8-GLIS3* fusion gene in HTTs and other thyroid neoplasms of the control cohort determined by RT-PCR (bottom). AC: anaplastic carcinomas; FA: follicular adenomas; FC: follicular carcinomas; HCT: Hurthle cell tumors; HTT: hylinizing trabecular tumors; MC: medullary carcinomas; PDC: poorly differentiated carcinomas; PTC: papillary thyroid carcinomas. **F)** Frequency of *PAX8-GLIS3* fusion gene in HTTs analyzed in this study and by Nikiforova et al., and other neoplasms as reported by TCGA fusion gene database. Hyalinizing trabecular tumor (HTT), Adrenocortical carcinoma (ACC), bladder urothelial carcinoma (BLCA), breast invasive carcinoma (BRCA), cervical squamous cell carcinoma and endocervical adenocarcinoma (CESC), cholangiocarcinoma (CHOL), colon adenocarcinoma (COAD), lymphoid neoplasm diffuse large B-cell lymphoma (DLBC), esophageal carcinoma (ESCA), glioblastoma multiforme (GBM), head and neck squamous cell carcinoma (HNSC), kidney chromophobe (KICH), kidney renal clear cell carcinoma (KIRC), kidney renal papillary cell carcinoma (KIRP), acute myeloid leukemia (LAML), brain lower grade glioma (LGG), liver hepatocellular carcinoma (LIHC), lung adenocarcinoma (LUAD), lung squamous cell carcinoma (LUSC), mesothelioma (MESO), ovarian serous cystadenocarcinoma (OV), pancreatic adenocarcinoma (PAAD), pheochromocytoma and paraganglioma (PCPG), prostate adenocarcinoma (PRAD), rectum adenocarcinoma (READ), sarcoma (SARC), skin cutaneous melanoma (SKCM), stomach adenocarcinoma (STAD), testicular germ cell tumors (TGCT), thyroid carcinoma (THCA), thymoma (THYM), uterine corpus endometrial carcinoma (UCEC), uterine carcinosarcoma (UCS), uveal melanoma (UVM).

Figure 5. Co-occurrence of a PTC and an HTT in a single patient. The scanned histological section contains a small PTC (2 mm, upper right corner of the scanned slide, dashed circle line) and a HTT (main lesion, dashed semicircular line). FISH was performed and selected fields were scanned within the two lesions, thus demonstrating *PAX8-GLIS3* fusions in the HTT (**A**, **B**), whereas no rearrangements were appreciated in the PTC (**C**, **D**).

Figure 1

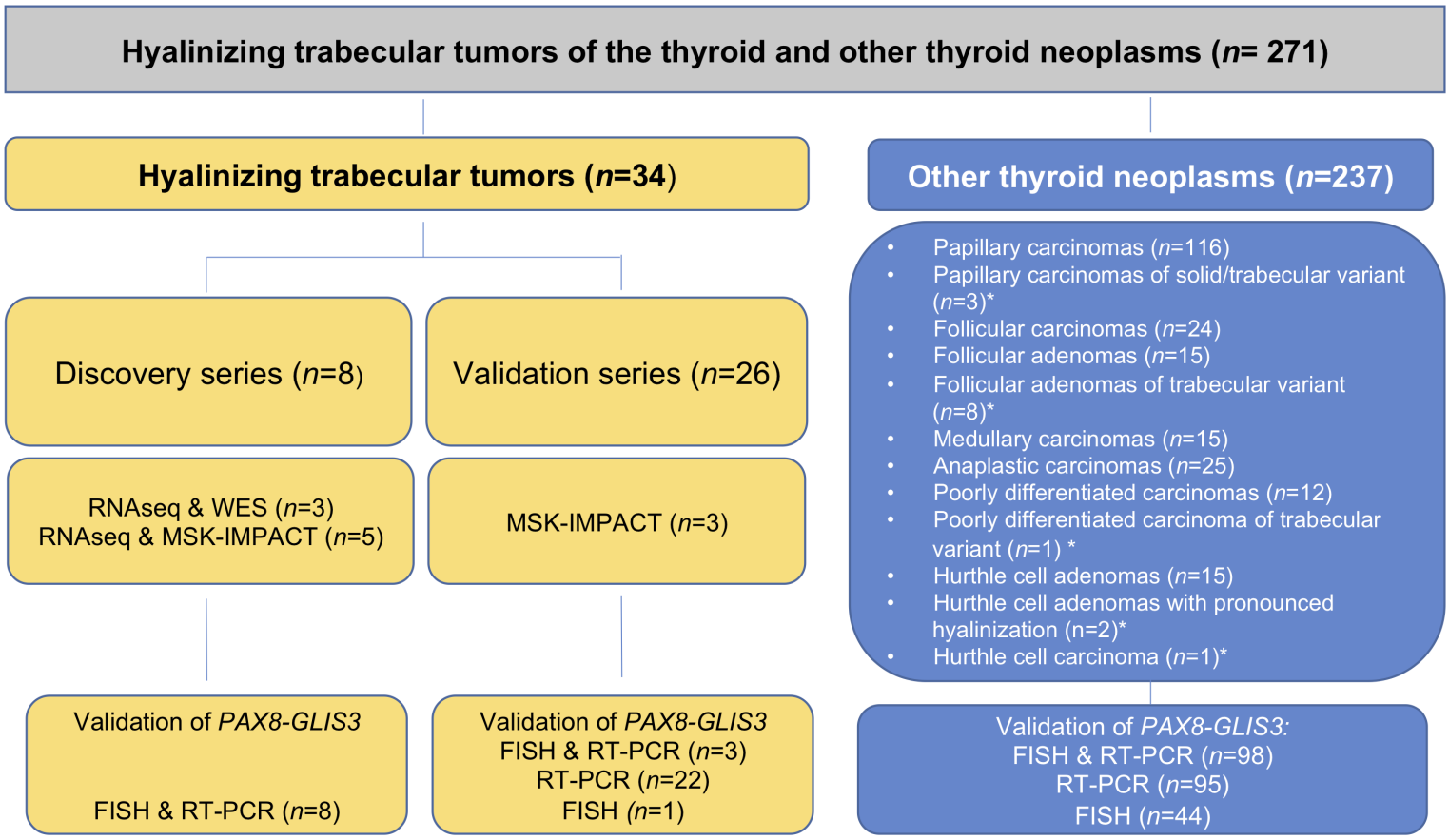
Hyalinizing trabecular tumors of the thyroid and other thyroid neoplasms (n= 271)
Hyalinizing trabecular tumors (n=34)
Other thyroid neoplasms (n=237)
Discovery series (n=8)
Validation series (n=26)
RNAseq & WES (n=3)
RNAseq & MSK-IMPACT (n=5)
MSK-IMPACT (n=3)
Validation of PAX8-GLIS3
FISH & RT-PCR (n=8)
Validation of PAX8-GLIS3
FISH & RT-PCR (n=3)
RT-PCR (n=22)
FISH (n=1)
Papillary carcinomas (n=116)
Papillary carcinomas of solid/trabecular variant (n=3)*
Follicular carcinomas (n=24)
Follicular adenomas (n=15)
Follicular adenomas of trabecular variant (n=8)*
Medullary carcinomas (n=15)
Anaplastic carcinomas (n=25)
Poorly differentiated carcinomas (n=12)
Poorly differentiated carcinoma of trabecular variant (n=1) *
Hurthle cell adenomas (n=15)
Hurthle cell adenomas with pronounced hyalinization (n=2)*
Hurthle cell carcinoma (n=1)*
Validation of PAX8-GLIS3:
FISH & RT-PCR (n=98)
RT-PCR (n=95)
FISH (n=44)

Figure 2

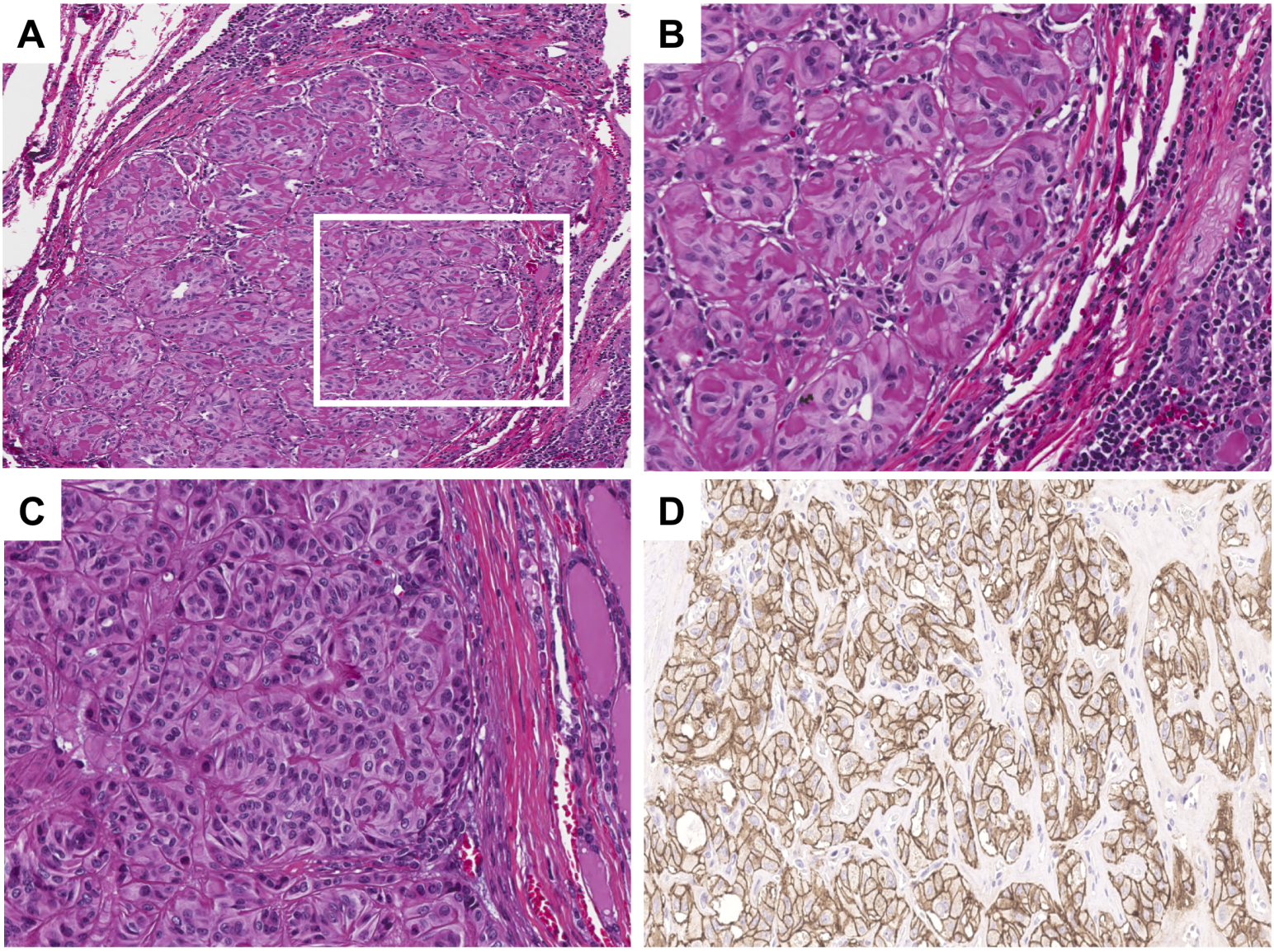

Figure 3

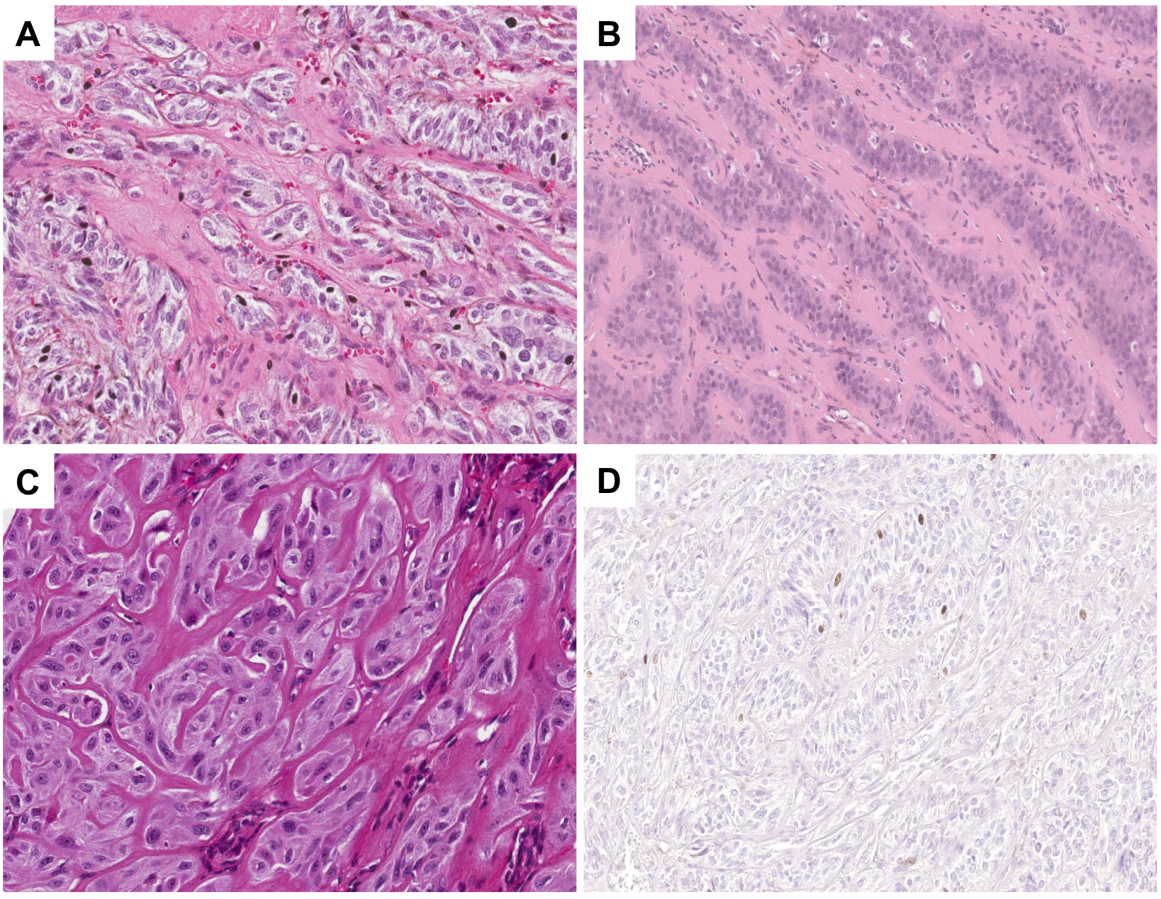

Figure 4

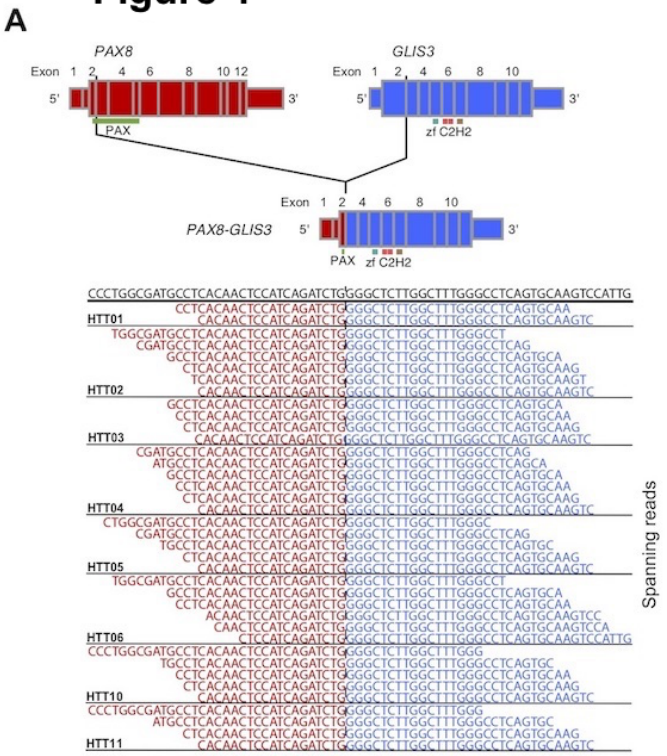
A
PAX8
GLIS3
PAX8-GLIS3
PAX
zf C2H2
Spanning reads
HTT01
HTT02
HTT03
HTT04
HTT05
HTT06
HTT10
HTT11

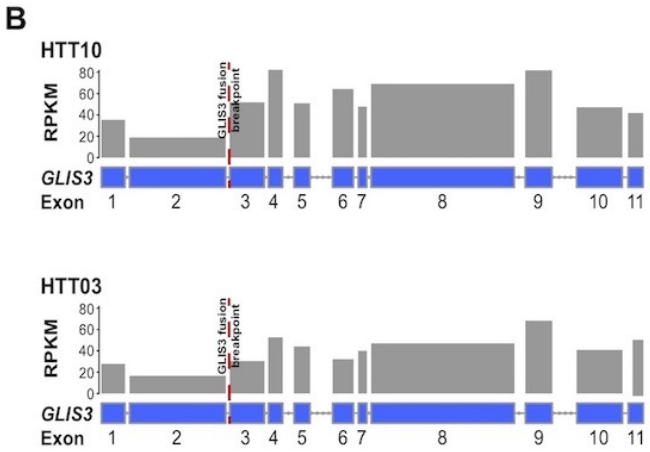
B
HTT10
HTT03
RPKM
GLIS3 fusion breakpoint
GLIS3
Exon

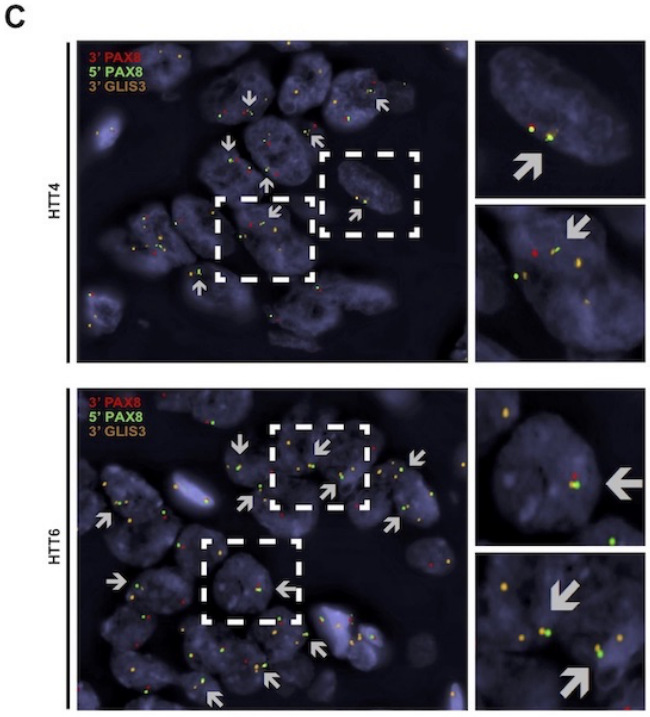
C
HTT4
HTT6
3' PAX8
5' PAX8
3' GLIS3

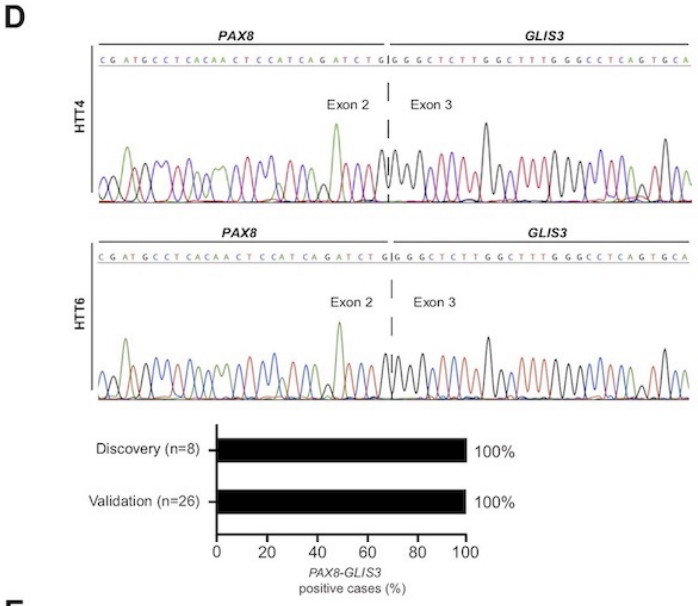
D
PAX8
GLIS3
HTT4
HTT6
Exon 2
Exon 3
Discovery (n=8)
Validation (n=26)
100%
PAX8-GLIS3
positive cases (%)

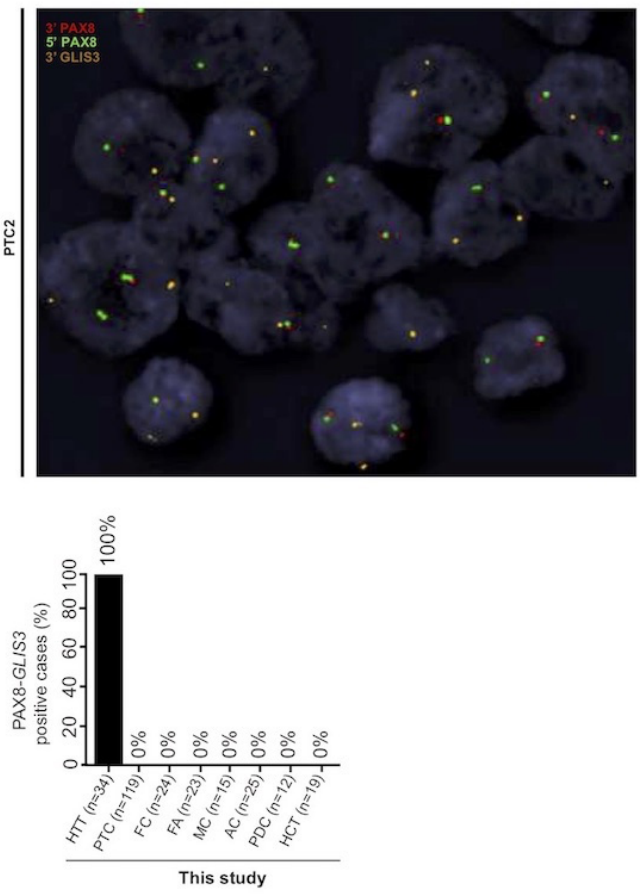
E
PTC2
3' PAX8
5' PAX8
3' GLIS3
PAX8-GLIS3
positive cases (%)
HTT (n=34)
PTC (n=119)
FC (n=24)
FA (n=23)
MC (n=15)
AC (n=25)
PDC (n=12)
HCT (n=19)
This study

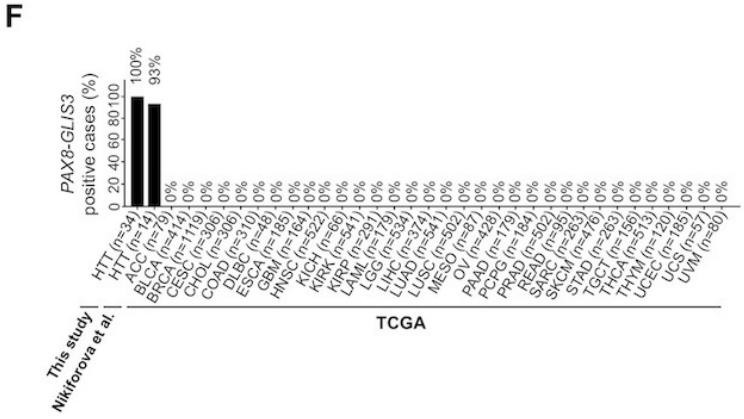
F
PAX8-GLIS3
positive cases (%)
This study
Nikiforova et al.
TCGA

Figure 5